
Can Artificial Intelligence Reliably Report Chest X-Rays?

Radiologist Validation of an Algorithm trained on 1.2 Million X-Rays

Preetham Putha¹, Manoj Tadepalli¹, Bhargava Reddy¹, Tarun Raj¹, Justy Antony Chiramal¹, Shalini Govil², Namita Sinha², Manjunath KS², Sundeep Reddivari², Pooja Rao¹, and Prashant Warier¹

¹Qure.ai, Mumbai, IN

²Columbia Asia Radiology Group, Bangalore, IN

Abstract

Background and Objectives Chest x-rays are the most commonly performed, cost-effective diagnostic imaging tests ordered by physicians. A clinically validated, automated artificial intelligence system that can reliably separate normal from abnormal would be invaluable in addressing the problem of reporting backlogs and the lack of radiologists in low-resource settings. The aim of this study was to develop and validate a deep learning system to detect chest x-ray abnormalities.

Methods A deep learning system was trained on 1.2 million x-rays and their corresponding radiology reports to identify abnormal x-rays and the following specific abnormalities: blunted costophrenic angle, calcification, cardiomegaly, cavity, consolidation, fibrosis, hilar enlargement, opacity and pleural effusion. The system was tested versus a 3-radiologist majority on an independent, retrospectively collected de-identified set of 2000 x-rays. The primary accuracy measure was area under the ROC curve (AUC), estimated separately for each abnormality as well as for normal versus abnormal reports.

Results The deep learning system demonstrated an AUC of 0.93(CI 0.92-0.94) for detection of abnormal scans, and AUC (CI) of 0.94(0.92-0.97), 0.88(0.85-0.91), 0.97(0.95-0.99), 0.92(0.82-1), 0.94(0.91-0.97), 0.92(0.88-0.95), 0.89(0.84-0.94), 0.93(0.92-0.95), 0.98(0.97-1), 0.93(0.87-0.99) for the detection of blunted costophrenic angle, calcification, cardiomegaly, cavity, consolidation, fibrosis, hilar enlargement, opacity and pleural effusion respectively.

Conclusions and Relevance Our study shows that a deep learning algorithm trained on a large quantity of well-labelled data can accurately detect abnormalities on chest x-rays. As these systems further increase in accuracy, the feasibility of using artificial intelligence to extend the reach of chest x-ray interpretation and improve reporting efficiency will increase in tandem.

1 Introduction

Chest x-rays are the most commonly ordered diagnostic imaging tests, with millions of x-rays performed globally every year[1]. While the chest x-ray is frequently performed, interpreting a chest x-ray is one of the most subjective and complex of radiology tasks, with inter-reader agreement varying from a kappa value of 0.2 to 0.77, depending on the level of experience of the reader, the abnormality being detected and the clinical setting[2–5]. Due to their wide availability and affordability, chest x-rays are performed all over the world, including remote areas with few or no radiologists. In some parts of the world, digital chest x-ray machines are more widely available than personnel sufficiently trained to report the x-rays they generated[6, 7]. If automated detection can be applied in low-resource settings as a disease screening tool, the benefits to population health outcomes globally could be significant. An example of the use of chest x-rays as a screening tool is in tuberculosis screening, where chest x-rays, in the hands of expert readers, are more sensitive than clinical symptoms for the early detection of tuberculosis[8].

Over the last few years, there has been increasing interest in the use of deep learning algorithms to assist with abnormality detection on medical images[9–11]. This is a natural consequence of the rapidly growing ability of machines to interpret natural images and detect objects in them. On chest x-rays in particular, there have been a series of studies describing the use of deep learning algorithms to detect various abnormalities[12–14]. Most of these have been limited by the lack of availability of large, high-quality datasets with the largest published work describing an algorithm that has been trained on 112,120 x-rays [13, 14], a relatively small number considering that the majority of chest x-rays are normal, abnormal x-rays are less common and specific abnormalities being rarer still. The previously published work on deep learning for chest x-ray abnormality detection has not made a distinction between the diagnosis of ‘diseases’ and the detection of ‘abnormal findings’. Our approach was to focus on the detection of abnormalities on the x-ray that can be detected visually by an expert without the benefit of the clinical history. This would allow the system to be applied across geographies and differing disease prevalence.

In this paper, we describe the training and radiologist validation of a deep learning system to detect and identify chest x-ray abnormalities. We trained the system on 1.2 million x-rays and tested it against the majority vote of a panel of 3 radiologists on an independent dataset containing 2000 studies. Abnormalities on chest x-rays range from very small lesions to diffuse abnormalities that cover large parts of the lung. The optimal deep learning model architecture differs based on the abnormality being detected; hence, we developed and tested a system that uses an individual algorithm for each abnormality.

2 Methods

2.1 Algorithm Development

We used 1.2 million chest x-rays and their corresponding radiology reports to train convolutional neural networks (CNNs) to identify chest x-ray abnormality. We developed natural language processing (NLP) algorithms to parse unstructured radiology reports and extract information about the presence and nature of chest x-ray abnormality. These extracted findings were used as labels when training CNNs. Individual networks were trained to identify normal x-rays, and the following chest x-ray findings: ‘blunted CP angle’, ‘calcification’, ‘cardiomegaly’, ‘cavity’, ‘consolidation’, ‘fibrosis’, ‘hilar enlargement’, ‘opacity’ and ‘pleural effusion’.

2.1.1 Pre-processing and Data Augmentation

The training dataset was obtained from 27 centers, and contained chest x-rays that varied considerably in size, resolution and quality. All x-rays were down-sampled and resized to a standard size. A set of image normalization techniques was applied to these images to reduce source-dependent variation. Additionally, a number of abnormality-specific data augmentation techniques were applied. The aim of data augmentation is to generate a dataset that can be used to train models so they are unaffected by variability in x-ray machine manufacturer, model, voltage, exposure and other parameters that vary from center to center.

2.1.2 Architecture and Training

The basic blocks in the systems that detect individual abnormalities are versions of densenets[15] or resnets[16] that are modified to process information at a significantly higher resolution than their vanilla versions. All the classification models that build up the individual abnormality detection systems are pre-trained on the task of separating chest x-rays from x-rays of other body parts rather than the popular ImageNet pre-training. This step is aimed at making use of the super-set consisting of all the x-rays. We observed improved model convergence and incremental gains in generalization performance when compared to ImageNet pre-training.

2.1.3 Use of Model Ensembles

Ensembling is a simple way of improving generalization performance by combining the predictions produced by a set of models. Multiple models are trained to detect each abnormality. These models differ with respect to the architecture used, model initialization conditions and the distribution of the training dataset. A subset of these models is selected using various heuristics[17] and a majority

X-Ray Pool	Center	Date
Pool 1	CAH-Salt Lake	16-08-2017 to 31-08-2017
	CAH-Pune	07-09-2017 to 23-09-2017
	CAH-Mysore	10-07-2017 to 25-07-2017
Pool 2	CAH-Pune	1-02-2013 to 31-07-2013

Table 1: Source of x-rays used for the study

ensembling scheme is used to combine the predictions of these selected models to make a decision about the presence or absence of a particular abnormality.

2.2 Study Design

2.2.1 Data selection

A combination of out-patient and in-hospital x-rays from three Columbia Asia Hospitals (CAH) in India at Kolkata, Pune and Mysore were used to create two databases for the study, as described in Table 1. There was no overlap between these centers or the centers from where training data was obtained.

All data were de-identified before use in this study. Radiologist validation was performed in 2 phases, using a separate set of 1000 x-rays for each phase. Sample size calculations are explained in section 2.4.1. Chest x-rays were filtered as follows: all PA and AP view chest x-rays where a corresponding radiologist report was available were selected. From this set, x-rays from pediatric patients (< 14 years of age) and x-rays taken with the patient in the supine position (bedside/ portable x-rays) were excluded. A set of 1000 x-rays (Set 1) was then selected randomly from Pool 1, with no enrichment of x-rays containing the abnormalities of interest. A second set of 1000 x-rays (Set 2) were sampled from Pool 2 to include a minimum of 80 examples of each abnormality and a random sample of the remaining x-rays. We used an NLP tool that parsed the x-ray radiology reports to implement the exclusions listed above, and to automate the sampling for phase 2. The study design is illustrated in Figure 1.

2.2.2 Inclusion and Exclusion criteria

PA and AP view chest x-rays from ambulatory adult patients taken in the standing position were included in the study. x-rays from patients under 14 years of age, x-rays taken in the supine position - from bedside or portable x-ray machines - were excluded. As a result, the datasets did not contain any x-rays with visible intravenous lines, tubes, catheters, ECG leads or any implanted medical devices such as pacemakers.

2.2.3 Abnormality definitions

To ensure that reviewing radiologists and the algorithm were using the same frame of reference for defining abnormalities, the definitions in Table 2.2 were used to extract tags from reports during the algorithm development phase and by the radiologists during the validation phase.

2.3 Validation of NLP algorithm and deep learning algorithms

2.3.1 Abnormality extraction from reports

We used a custom NLP to extract relevant findings from the original radiology reports. The NLP algorithm was constructed using a thoracic imaging glossary [18], curated by a panel of radiologists and combined with standard NLP tools to manage typographic errors, detect negations and identify synonyms. The custom NLP algorithm was iterated through trial and error and its accuracy checked on an independent dataset of 1000 chest x-rays against an expert reader who was provided with the tag definitions (2), original reports and the corresponding x-rays. These expert readers were blinded to the algorithm output.

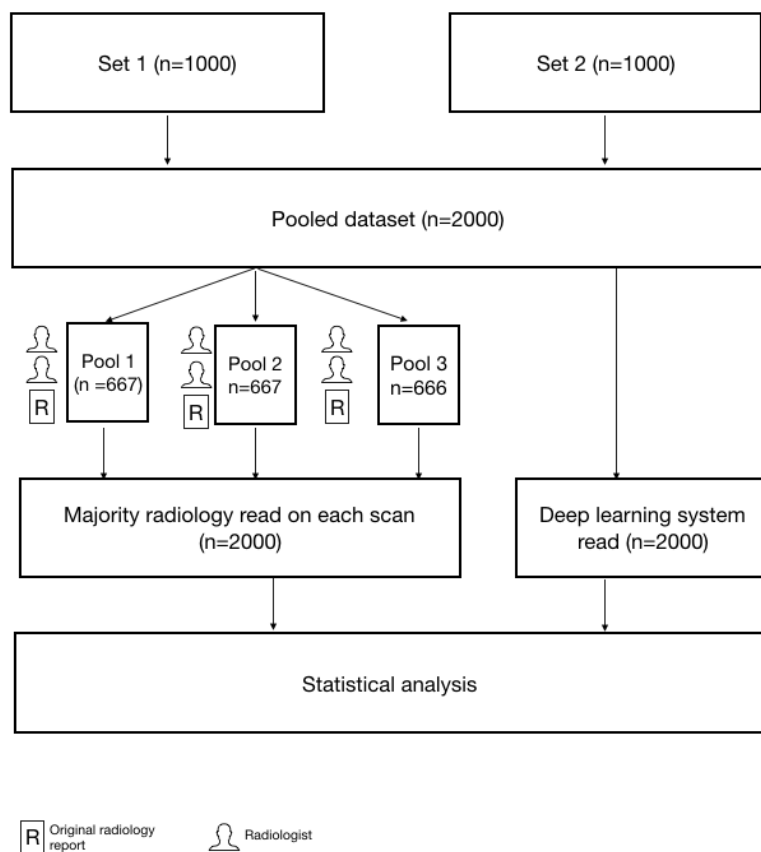


Figure 1: Study Design.

2.3.2 Validation of deep learning algorithm: accuracy of abnormality detection

The x-rays were randomly divided among six certified radiologists (three pairs), with 3-15 years of radiology experience. A third read was available in the form of the original radiology report accompanying each chest x-ray. A custom validation portal was used for radiologist validation and contained the original resolution DICOM file. Radiologists marked ‘present’ or ‘absent’ for each abnormality. A pen tool was used to mark out the area affected and a text field was available for comments. The gold standard for this study was the majority opinion on the presence or absence of each abnormality between three radiologists’ reads. Algorithm accuracy on detecting abnormal x-rays and on each individual abnormality is reported versus this gold standard. Algorithm output was generated on both datasets and placed in a locked database, until completion of the radiologist validation. Radiologists were blinded to the original x-ray report and the algorithm output when reviewing the x-rays for the validation study.

2.4 Statistical Analysis

2.4.1 Sample size calculation

Calculating sensitivity and specificity precisely with a 95% confidence interval would require a sample size of approximately 20,000 in an un-enriched dataset randomly sampled from the population. We therefore used the enrichment strategy detailed in Section 2.2.1. The sample size required for estimating 80% sensitivity with 90% accuracy and 95% confidence interval is 951. Therefore, 2000 x-rays were considered sufficient to evaluate the classification of x-rays as normal or abnormal. Sensitivity was chosen over specificity for this sample size calculation as a false negative result is considered a worse outcome than a false positive in preliminary diagnostic investigations [19]. The

Finding	Definition for tag extraction from radiology reports	Definition for radiologist review
Normal	‘No abnormality detected’ or ‘Normal’	Normal x-ray
Blunted CP angle	Blunted CP angle	CP angle blunted/obscured: pleural effusion/pleural thickening
Calcification	Calcification	Any calcification including:aortic arch calcification/costal cartilage calcification/calcified pulmonary density/ microcalcification
Cardiomegaly	Cardiomegaly	CTR(cardiothoracic ratio) > 0.5
Cavity	Pulmonary cavity	Pulmonary cavity
Consolidation	Consolidation/ pneumonia/ air-bronchogram	Pulmonary consolidation
Fibrosis	Fibrosis	Lung fibrosis/ interstitial fibrosis/ fibrocavitary lesion
Hilar prominence	Hilar enlargement/ prominent hilum/ hilar lymphadenopathy	Enlarged hilum/ prominent hilum/ hilar lymphadenopathy
Opacity	Lung opacity/ opacities/ shadow/ density/ infiltrate, consolidation/ mass/ nodule/ pulmonary calcification/ fibrosis	Any lung opacity/ multiple opacities including: infiltrate/ consolidation/ mass/ nodule/ pulmonary calcification/ fibrosis Note: pleural abnormalities not included under this tag
Pleural Effusion	Pleural Effusion	Pleural Effusion

Table 2: Abnormality definitions

abnormalities we studied have a prevalence of less than 5% in the typical outpatient setting. A sample size of 951 x-rays would give 3% precision for estimating 80% specificity at 95% confidence interval. Given a prevalence of less than 10% for each of the specific conditions listed above, at least 77 true cases per condition would give a sensitivity of 80% with 10% precision and 95% confidence interval. Therefore, we used a minimum of 80 true cases per condition for Set 2.

2.4.2 Algorithm performance measurements versus radiologists

When calculating AUC for a particular abnormality, we used Set 1 in its entirety and all x-rays positive for that abnormality from Set 2. This allowed us to use a sufficiently large number of ‘abnormality-positive’ cases for sensitivity calculation, while keeping the ratio of normal to abnormal x-rays close to the natural distribution. This also enabled a fairer estimation of specificity than using both sets combined and was equivalent to evaluating the accuracy of detection for each abnormality separately. The entire dataset ($n = 2000$) was used when calculating AUC for detection of abnormal x-rays. We calculated AUC confidence intervals using the ‘distribution-based’ method described by Hanley and McNeil [20]. We measured the concordance between paired readers for each abnormality with percentage of agreement and the Cohen’s kappa(κ) statistic[21]. In addition, we measured concordance between all three readers for each finding using Fleiss’ kappa(κ) [22] statistic. Since readers were grouped into three pairs, each reported measure of inter-reader agreement is the average of three estimates.

3 Results

Basic demographics and the number of scans containing each abnormality are summarized in table 4. 658 out of 2000 x-rays were abnormal, with the most frequent abnormalities being ‘opacity’,

Table 3: Demographics of the study population

Characteristic	Set1 (<i>n</i> = 1000)	Set2 (<i>n</i> = 1000)	Combined (<i>n</i> = 2000)
PATIENT DEMOGRAPHICS			
Age			
No. of scans for which age was known	803	1000	1803
Mean	48.04	50.61	49.32
Standard deviation	18.69	17.93	18.36
Range	16 – 95	16 – 100	16 – 100
No. of females / No. of scans for which sex was known (percentage)	324/803 (40.3%)	265/1000 (26.5%)	589/1803 (32.6%)
PREVALENCE			
No. of scans (percentage) with			
No abnormality detected(Normal)	440	218	658
Blunted CP angle	35	121	156
Calcification	57	244	301
Cardiomegaly	61	116	177
Cavity	1	15	16
Consolidation	13	92	105
Fibrosis	13	97	110
Hilar enlargement	15	49	64
Opacity	104	341	445
Pleural Effusion	36	122	158

Table 4: Demographics of the study population Based on a 3-reader consensus ground truth derived from original radiology report plus consensus of radiologists, as defined in section 2.2.3

‘cardiomegaly’ and ‘calcification’. There were not enough x-rays with ‘cavity’ to confidently calculate the accuracy of the deep learning system in identifying this abnormality.

Achieving a high accuracy on report parsing enabled the use of a large number of x-rays to train the deep learning algorithms. Abnormality extraction accuracy from radiology reports versus manual extraction by a single reader is summarized in Table 5a. The algorithm was able to detect normal x-ray reports with a sensitivity of 0.94 and a specificity of 1 versus the expert reader. For detection of individual abnormalities from reports, sensitivity varied from 0.93 for pleural effusion to 1 for calcification and cavity; specificity varied from 0.92 for opacity to 0.99 for fibrosis.

3.1 Interradiologist Concordance

Inter-reader concordance is described in Table 5b. Concordance was highest on detection of abnormal x-rays (inter-reader agreement 85%, Cohen’s kappa 0.6, Fleiss’ kappa 0.56) and on the specific abnormalities pleural effusion (inter-reader agreement 85%, Cohen’s kappa 0.6, Fleiss’ kappa 0.56), cardiomegaly (inter-reader agreement 85%, Cohen’s kappa 0.6, Fleiss’ kappa 0.56), and calcification (inter-reader agreement 85%, Cohen’s kappa 0.6, Fleiss’ kappa 0.56).

3.2 Algorithm accuracy versus the majority opinion of 3 radiologists

The deep learning system accuracy at identifying each of the 12 abnormalities is listed in table 6. 2 shows ROC curves for each abnormality, plotted on the entire dataset (*n* = 2000) versus the majority opinion of 3 radiologists, drawn randomly out of a pool of 6 radiologists. Individual radiologist sensitivity and specificity for the 6 radiologists is marked on each plot. In most cases, individual radiologist sensitivity and specificity was marginally above the ROC curve, with exceptions for pleural effusion, cardiomegaly and opacity where algorithm performance was equal to the performance of some individuals.

Finding	#Positives	Sensitivity (95% CI)	Specificity (95% CI)
Normal(No abnormality detected)	105	0.9429 (0.8798-0.9787)	1.0000 (0.9959-1.0000)
Blunted CP angle	146	0.9795 (0.9411-0.9957)	0.9824 (0.9712-0.9901)
Calcification	116	1.0000 (0.9687-1.0000)	0.9660 (0.9519-0.9770)
Cardiomegaly	125	0.9920 (0.9562-0.9998)	0.9760 (0.9635-0.9851)
Cavity	30	1.0000 (0.8843-1.0000)	0.9856 (0.9759-0.9921)
Consolidation	161	0.9876 (0.9558-0.9985)	0.9761 (0.9634-0.9854)
Fibrosis	124	0.9839 (0.9430-0.9980)	0.9931 (0.9851-0.9975)
Hilar Enlargement	289	0.9689 (0.9417-0.9857)	0.9732 (0.9585-0.9838)
Opacity	612	0.9608 (0.9422-0.9747)	0.9251 (0.8942-0.9492)
Pleural Effusion	246	0.9309 (0.8917-0.9592)	0.9602 (0.9436-0.9730)
Total(all findings)	1954	0.9672 (0.9584-0.9747)	0.9771 (0.9736-0.9803)

(a) Tag extraction accuracy: performance of the NLP algorithm in inferring findings from the reports.

Finding	Radiologist 1 & 2		All reads
	Agreement %	Cohen's κ	Fleiss' κ
Normal(No abnormality detected)	85.00	0.6049	0.5618
Blunted CP angle	83.58	0.2968	0.3054
Calcification	83.00	0.5803	0.5821
Cardiomegaly	91.60	0.5333	0.5284
Cavity	97.50	0.3824	0.4047
Consolidation	88.28	0.3529	0.3397
Fibrosis	89.40	0.3781	0.3495
Hilar Enlargement	89.38	0.2630	0.2101
Opacity	70.70	0.2306	0.1733
Pleural Effusion	90.69	0.5341	0.5305

(b) Concordance between the readers.

Table 5: Reliability of the gold standard: Abnormality extraction accuracy from radiology reports versus manual extraction by a single reader is summarized in table 5a. Inter-reader concordance is described in table 5b

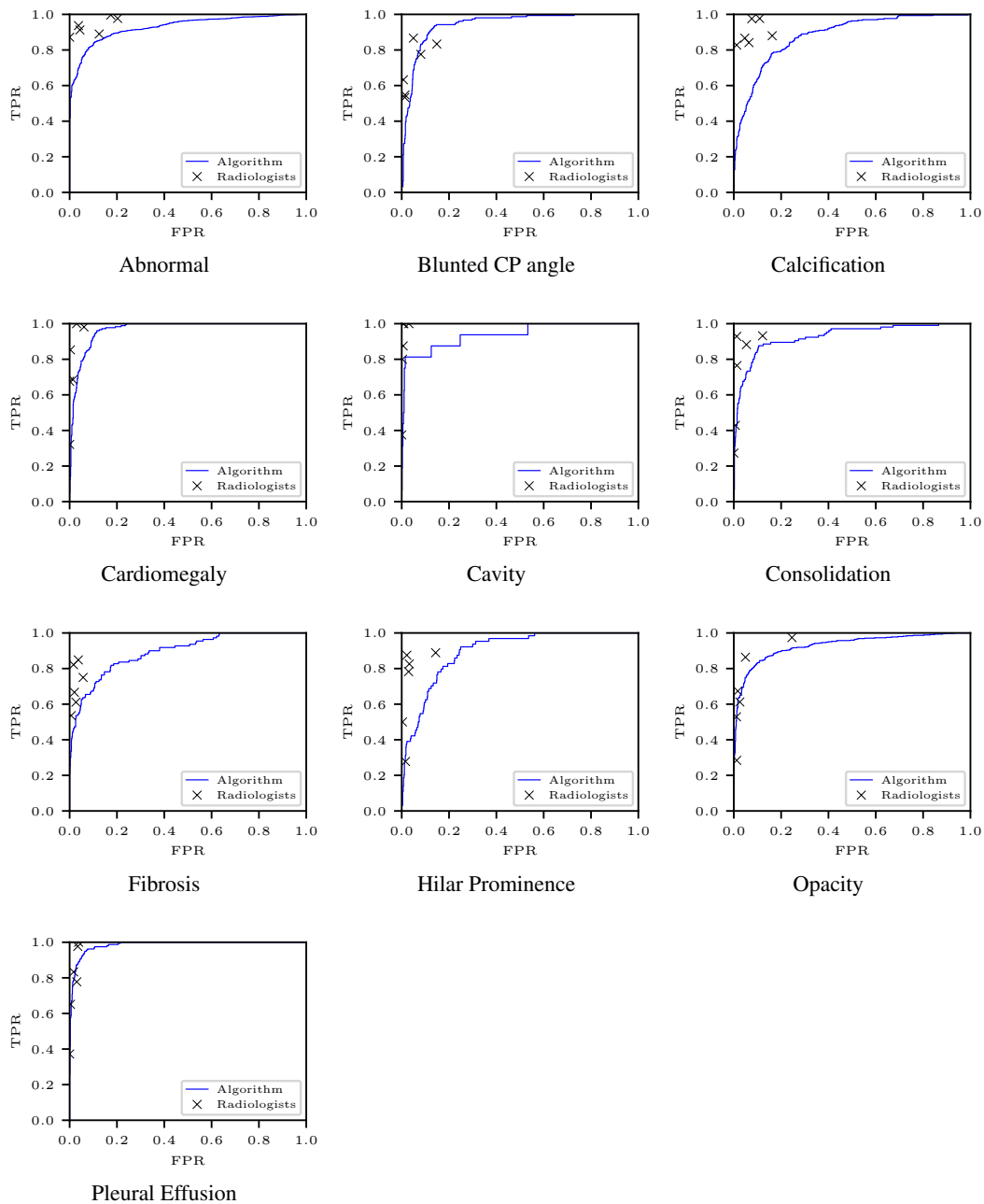


Figure 2: AUC curves for all abnormalities versus a 3-radiologist majority, with reader performance marked.

Finding	AUC (95% CI)	High sensitivity operating point		High specificity operating point	
		Sensitivity	Specificity	Sensitivity	Specificity
Normal(No Abnormality Detected)	0.9278 (0.9162-0.9394)	0.9100	0.7519	0.8192	0.9086
Blunted CP angle	0.9434 (0.9179-0.9690)	0.9487	0.7692	0.8461	0.9100
Calcification	0.8812 (0.8550-0.9073)	0.9069	0.6550	0.6511	0.8912
Cardiomegaly	0.9670 (0.9484-0.9856)	0.9717	0.8636	0.8474	0.9284
Cavity	0.9351 (0.8511-1.0000)	0.9375	0.7528	0.8125	0.9850
Consolidation	0.9394 (0.9074-0.9714)	0.9047	0.7921	0.8285	0.9049
Fibrosis	0.9171 (0.8810-0.9532)	0.9000	0.7072	0.7818	0.9011
Hilar Enlargement	0.8908 (0.8379-0.9437)	0.9218	0.7509	0.6718	0.8907
Opacity	0.9324 (0.9155-0.9493)	0.9033	0.7836	0.8000	0.9011
Pleural Effusion	0.9841 (0.9703-0.9979)	0.9810	0.8355	0.8797	0.9660

Table 6: Performance of the algorithms

4 Discussion

Long before deep learning, automated chest x-ray interpretation using traditional image processing methods have been used to identify chest-ray views, segment parts of the lung, identify cardiomegaly or lung nodules and diagnose tuberculosis. However, these traditional methods did not come into routine clinical use because of their need for standardized x-ray quality, machine model and images free of artefacts[23–28]. With the advent of convolutional neural networks and deep learning, there has been a resurgence of interest in automated chest x-ray interpretation with many research groups leveraging convolutional neural networks to detect pneumonia, tuberculosis and other chest diseases[12–14, 29–31].

In 2017, Shin et al. [12] used a combination of convolutional neural networks and recurrent neural networks to identify, caption and describe the context of chest x-ray abnormalities, but were limited by the small size of training datasets that were publicly available. Subsequently, Lakhani and Sundaram [29] trained convolutional neural networks to detect tuberculosis and reported an AUC of 0.99 that was achieved with a small training dataset of 857 x-rays and a test dataset of 150 x-rays. This exceptionally high accuracy has not been replicated by any other group. In 2017, Wang et al. [30] used the Chestx-ray14 dataset, a single-source dataset containing 112,120 x-rays and NLP-generated labels for 14 thoracic diseases that was made publicly available by the NIH. They used this dataset to train and validate deep learning algorithms with NLP-generated labels as ground truth and reported AUCs ranging from 0.69 to 0.91 for various abnormalities[13, 14, 30, 31]. Using the same Chestx-ray14 dataset, Rajapurkar et al trained their algorithm ‘CheXNet’ to detect pneumonia and validated it against a dataset of 420 x-rays independently reported by Stanford Radiologists. They found that the algorithm outperformed Radiologists in detecting pneumonia[13]. The lack of large, reliable, openly available chest x-ray datasets with radiologist-confirmed ground truth makes it difficult to benchmark deep learning algorithms.

Ours is the largest chest x-ray training and testing dataset reported in the literature: we trained a deep learning algorithm on 1.2 million chest x-rays, and validated it against 2000 chest x-rays labelled by a 3-radiologist majority. For determining algorithm accuracy, the 2000 chest x-ray dataset was used, separate from the training dataset and sourced from a separate centre. The algorithm

achieved an AUC of 0.93 for differentiating normal from abnormal chest x-rays, while the AUC for detection of individual abnormalities varied from 0.86 to 0.98. AUCs were higher for abnormalities with higher prevalence in the dataset, greater inter-reader agreement and consistency of reporting terminology. The highest accuracy was achieved for findings that were unambiguously defined and reported with consistent terminology, such as pleural effusion or cardiomegaly. Unlike previous algorithms trained to make a diagnosis, our chest x-ray algorithm was trained to identify abnormal findings and differentiate normal from abnormal. We did this to facilitate clinical use of the algorithm across geographies, independent of local disease prevalence.

Physician concordance, sensitivity and specificity of chest x-ray interpretations are known to vary widely depending on the abnormality being detected, reader expertise, and clinical setting. Inter-radiologist agreement on interpretation of adult chest x-rays with pneumonia ranges from a kappa value (κ) of 0.43 to 0.53 [2, 3]. For asbestos-related abnormalities on chest x-rays, inter-reader agreement was fair ($\kappa=0.36$), with the highest agreement on pleural calcification ($\kappa=0.63$) [32]. Studies on the radiological assessment of tuberculosis showed moderate intra-observer concordance with $\kappa=0.55$ on average, increasing to 0.64 for abnormalities requiring urgent attention [33]; similar concordance was observed for TB screening in patients with HIV $\kappa=0.63$ [34]. In contrast, inter-reader agreement on pediatric hilar lymphadenopathy ranged from values of 0.05 to 0.55 [35]. The inter-reader variability we encountered in our study is similar to that previously documented. However, for the detection of blunted CP angle, we found lower agreement rate ($\kappa=0.3$) than previously been reported ($\kappa=0.7$) [36]. Agreement rates for opacity are also low in our study, likely related to differences in reader definition of ‘opacity’. Our readers were blinded to clinical history, a factor that might have impacted both accuracy and inter-reader variance. Experience did not reduce inter-reader variance, suggesting that the high inter-reader variance is due to the inherent difficulty in interpreting a 2D greyscale display of a 3D complex body part containing tissue densities that range from air to bone.

Radiologist opinion is not the ground truth for chest x-rays but is only a precursor to the final clinical and histopathology diagnosis. We tested the algorithm to determine if it can replicate radiologist observation of abnormality on chest x-rays rather than diagnose chest pathology. Although reader consensus is the customary mode of establishing ground truth in radiology, it does not provide information on inter-reader variability [37, 38]. We used a 3-reader majority opinion, without consensus, as ground truth. Our results demonstrate that manually curated, but fully automated NLP methods can be used to reliably detect abnormal findings in radiology reports at the scale required for training deep learning algorithms. However, chest x-ray reports are inherently subjective to differing reporting styles and are not optimized for automated extraction. The main limitation to sample size when using a 3-reader validation is radiologist time. We used an enriched data subset in an attempt to achieve adequate representation of each abnormality. This was achieved for all abnormalities except for ‘cavity’, where we could not reliably estimate algorithm accuracy. In our study, we did not exclude multiple x-rays from the same patient; however given that bedside and portable x-rays were excluded, the probability that repeated x-rays from the same patient occurred in the validation dataset is very low.

5 Conclusion

Our study demonstrates that deep learning algorithms trained on large datasets can accurately detect abnormalities on chest x-rays, with close to radiologist-level accuracy. Apart from providing automated chest x-ray interpretations in under-served and remote locations, automated draft or preliminary reports of abnormal chest x-rays can improve turnaround and clear backlogs. Further research is required to assess the clinical acceptance of artificial intelligence in the real-world and quantify the benefit of such automation to physicians and their patients.

References

- [1] NHS England. Diagnostic imaging dataset statistical release. *London: Department of Health*, 2017.
- [2] Diana Carolina Moncada, Zulma Vanessa Rueda, Antonio Macías, Tatiana Suárez, Héctor Ortega, and Lázaro Agustín Vélez. Reading and interpretation of chest x-ray in adults with

- community-acquired pneumonia. *The Brazilian Journal of Infectious Diseases*, 15(6):540–546, 2011.
- [3] RM Hopstaken, T Witbraad, JMA Van Engelshoven, and GJ Dinant. Inter-observer variation in the interpretation of chest radiographs for pneumonia in community-acquired lower respiratory tract infections. *Clinical radiology*, 59(8):743–752, 2004.
- [4] Boniface Moifo, Eric Walter Pefura-Yone, Georges Nguefack-Tsague, Marie Laure Gharingam, Jean Roger Moulion Tapouh, André-Pascal Kengne, and Samuel Nko’o Amvene. Inter-observer variability in the detection and interpretation of chest x-ray anomalies in adults in an endemic tuberculosis area. *Open Journal of Medical Imaging*, 5(03):143, 2015.
- [5] Shinsaku Sakurada, Nguyen TL Hang, Naoki Ishizuka, Emiko Toyota, Le D Hung, Pham T Chuc, Luu T Lien, Pham H Thuong, Pham TN Bich, Naoto Keicho, et al. Inter-rater agreement in the assessment of abnormal chest x-ray findings for tuberculosis between two asian countries. *BMC infectious diseases*, 12(1):31, 2012.
- [6] X-ray detector market by type (fpd, csi, gadox, ccd, line scan), panel (small, large), portability (fix, portable), digital system (new, retrofit), application (medical, orthopedic, mammogram, dental, security, industrial, ndt) - forecast to 2022. 2017.
- [7] Nigel Crisp and Lincoln Chen. Global supply of health professionals. *New England Journal of Medicine*, 370(10):950–957, 2014.
- [8] World Health Organization et al. Chest radiography in tuberculosis detection: summary of current who recommendations and guidance on programmatic approaches. Technical report, World Health Organization, 2016.
- [9] Varun Gulshan, Lily Peng, Marc Coram, Martin C Stumpe, Derek Wu, Arunachalam Narayanaswamy, Subhashini Venugopalan, Kasumi Widner, Tom Madams, Jorge Cuadros, et al. Development and validation of a deep learning algorithm for detection of diabetic retinopathy in retinal fundus photographs. *Jama*, 316(22):2402–2410, 2016.
- [10] Andre Esteva, Brett Kuprel, Roberto A Novoa, Justin Ko, Susan M Swetter, Helen M Blau, and Sebastian Thrun. Dermatologist-level classification of skin cancer with deep neural networks. *Nature*, 542(7639):115, 2017.
- [11] Sasank Chilamkurthy, Rohit Ghosh, Swetha Tanamala, Mustafa Biviji, Norbert G Campeau, Vasantha Kumar Venugopal, Vidur Mahajan, Pooja Rao, and Prashant Warier. Development and validation of deep learning algorithms for detection of critical findings in head ct scans. *arXiv preprint arXiv:1803.05854*, 2018.
- [12] Hoo-Chang Shin, Kirk Roberts, Le Lu, Dina Demner-Fushman, Jianhua Yao, and Ronald M Summers. Learning to read chest x-rays: Recurrent neural cascade model for automated image annotation. In *Proceedings of the IEEE conference on computer vision and pattern recognition*, pages 2497–2506, 2016.
- [13] Pranav Rajpurkar, Jeremy Irvin, Kaylie Zhu, Brandon Yang, Hershel Mehta, Tony Duan, Daisy Ding, Aarti Bagul, Curtis Langlotz, Katie Shpanskaya, et al. Chexnet: Radiologist-level pneumonia detection on chest x-rays with deep learning. *arXiv preprint arXiv:1711.05225*, 2017.
- [14] Zhe Li, Chong Wang, Mei Han, Yuan Xue, Wei Wei, Li-Jia Li, and F Li. Thoracic disease identification and localization with limited supervision. *arXiv preprint arXiv:1711.06373*, 2017.
- [15] Gao Huang, Zhuang Liu, Kilian Q Weinberger, and Laurens van der Maaten. Densely connected convolutional networks. In *Proceedings of the IEEE conference on computer vision and pattern recognition*, volume 1, page 3, 2017.
- [16] Kaiming He, Xiangyu Zhang, Shaoqing Ren, and Jian Sun. Deep residual learning for image recognition. In *Proceedings of the IEEE conference on computer vision and pattern recognition*, pages 770–778, 2016.
- [17] Rich Caruana, Alexandru Niculescu-Mizil, Geoff Crew, and Alex Ksikes. Ensemble selection from libraries of models. In *Proceedings of the twenty-first international conference on Machine learning*, page 18. ACM, 2004.
- [18] David M Hansell, Alexander A Bankier, Heber MacMahon, Theresa C McLoud, Nestor L Muller, and Jacques Remy. Fleischner society: glossary of terms for thoracic imaging. *Radiology*, 246(3):697–722, 2008.

- [19] Lisa M Schwartz, Steven Woloshin, Harold C Sox, Baruch Fischhoff, and H Gilbert Welch. Us women’s attitudes to false positive mammography results and detection of ductal carcinoma in situ: cross sectional survey. *Bmj*, 320(7250):1635–1640, 2000.
- [20] James A Hanley and Barbara J McNeil. The meaning and use of the area under a receiver operating characteristic (roc) curve. *Radiology*, 143(1):29–36, 1982.
- [21] Anthony J Viera, Joanne M Garrett, et al. Understanding interobserver agreement: the kappa statistic. *Fam Med*, 37(5):360–363, 2005.
- [22] Joseph L Fleiss. Measuring nominal scale agreement among many raters. *Psychological bulletin*, 76(5):378, 1971.
- [23] Zhiyun Xue, Daekeun You, Sema Candemir, Stefan Jaeger, Sameer Antani, L Rodney Long, and George R Thoma. Chest x-ray image view classification. In *Computer-Based Medical Systems (CBMS), 2015 IEEE 28th International Symposium on*, pages 66–71. IEEE, 2015.
- [24] Jeff Duryea and John M Boone. A fully automated algorithm for the segmentation of lung fields on digital chest radiographic images. *Medical Physics*, 22(2):183–191, 1995.
- [25] D Yousefian and V Mariano. Automated heart enlargement detection using chest x-ray image analysis. *Philippine Information Technology Journal*, 8(1):8–15, 2015.
- [26] Xin-Wei Xu, Takeshi Kobayashi, Heber MacMahon, Maryellen L Giger, et al. Development of an improved cad scheme for automated detection of lung nodules in digital chest images. *Medical Physics*, 24(9):1395–1403, 1997.
- [27] Stefan Jaeger, Alexandros Karargyris, Sema Candemir, Les Folio, Jenifer Siegelman, Fiona M Callaghan, Zhiyun Xue, Kannappan Palaniappan, Rahul K Singh, Sameer K Antani, et al. Automatic tuberculosis screening using chest radiographs. *IEEE Trans. Med. Imaging*, 33(2): 233–245, 2014.
- [28] Laurens Hogeweg, Clara I Sánchez, Pragnya Maduskar, Rick Philipsen, Alistair Story, Rodney Dawson, Grant Theron, Keertan Dheda, Liesbeth Peters-Bax, and Bram Van Ginneken. Automatic detection of tuberculosis in chest radiographs using a combination of textural, focal, and shape abnormality analysis. *IEEE transactions on medical imaging*, 34(12):2429–2442, 2015.
- [29] Paras Lakhani and Baskaran Sundaram. Deep learning at chest radiography: automated classification of pulmonary tuberculosis by using convolutional neural networks. *Radiology*, 284(2):574–582, 2017.
- [30] Xiaosong Wang, Yifan Peng, Le Lu, Zhiyong Lu, Mohammadhadi Bagheri, and Ronald M Summers. Chestx-ray8: Hospital-scale chest x-ray database and benchmarks on weakly-supervised classification and localization of common thorax diseases. In *Computer Vision and Pattern Recognition (CVPR), 2017 IEEE Conference on*, pages 3462–3471. IEEE, 2017.
- [31] Yaniv Bar, Idit Diamant, Lior Wolf, and Hayit Greenspan. Deep learning with non-medical training used for chest pathology identification. In *Medical Imaging 2015: Computer-Aided Diagnosis*, volume 9414, page 94140V. International Society for Optics and Photonics, 2015.
- [32] Elke Ochsmann, Tanja Carl, Peter Brand, Hans-Jürgen Raithel, and Thomas Kraus. Inter-reader variability in chest radiography and hrct for the early detection of asbestos-related lung and pleural abnormalities in a cohort of 636 asbestos-exposed subjects. *International archives of occupational and environmental health*, 83(1):39, 2010.
- [33] JP Zellweger, R Heinzer, M Touray, B Vidondo, and E Altpeter. Intra-observer and overall agreement in the radiological assessment of tuberculosis. *The International Journal of Tuberculosis and Lung Disease*, 10(10):1123–1126, 2006.
- [34] CS Kosack, S Spijker, J Halton, Maryline Bonnet, S Nicholas, K Chetcuti, A Mesic, WE Brant, Elizabeth Joekes, and S Andronikou. Evaluation of a chest radiograph reading and recording system for tuberculosis in a hiv-positive cohort. *Clinical radiology*, 72(6):519–e1, 2017.
- [35] GH Swingler, G Du Toit, S Andronikou, L Van der Merwe, and HJ Zar. Diagnostic accuracy of chest radiography in detecting mediastinal lymphadenopathy in suspected pulmonary tuberculosis. *Archives of disease in childhood*, 90(11):1153–1156, 2005.
- [36] Jean Bourbeau and Pierre Ernst. Between-and within-reader variability in the assessment of pleural abnormality using the ilo 1980 international classification of pneumoconioses. *American journal of industrial medicine*, 14(5):537–543, 1988.

- [37] Alexander A Bankier, Deborah Levine, Elkan F Halpern, and Herbert Y Kressel. Consensus interpretation in imaging research: is there a better way?, 2010.
- [38] Nancy A Obuchowski and Richard C Zepp. Simple steps for improving multiple-reader studies in radiology. *AJR. American journal of roentgenology*, 166(3):517–521, 1996.